# Total two-photon hadronic cross section and charm production cross section measurement with the L3 detector

VALERY P. ANDREEV[†]

*Department of Physics and Astronomy,*
*Louisiana State University,*
*Baton Rouge, LA 70803, USA*
*E-mail: Valeri.Andreev@cern.ch*

**Abstract**

We present the analysis of the reactions $e^+e^- \to e^+e^-\gamma^*\gamma^* \to e^+e^- hadrons$ and $e^+e^- \to e^+e^-\gamma^*\gamma^* \to e^+e^- c\bar{c}$ done by the L3 collaboration at 91, 130-140, 161-172 and 183 GeV energies. For the first reaction the cross sections $\sigma(e^+e^- \to e^+e^- hadrons)$ and $\sigma(\gamma\gamma \to hadrons)$ are measured in the interval $5 \leq W_{\gamma\gamma} \leq 145$ GeV. The diffractive production of the two $\rho^0$ mesons $\gamma\gamma \to \rho^0\rho^0$ is also studied at 183 GeV LEP energy. The observed slope of the rise of the $\sigma(\gamma\gamma \to hadrons)$ with energy is by factor two higher than expected from the universal Regge behaviour of total hadronic cross sections. The direct process $\gamma\gamma \to \mathrm{c\bar{c}}$ is found to be insufficient to describe the data for charm production. The measured charm production cross section values and event distributions require contributions from resolved processes, sensitive to the gluon density in the photon.

---

## 1 Introduction

The photon-photon interactions are studied at LEP $e^+e^-$ collider in a wide range of the centre-of-mass energies. The background from the annihilation events is normally very low. The $\gamma\gamma$ cross section is composed by a "soft VMD" interaction, which can be described by hadronic phenomenology, like the Regge poles, a point like two-photon reaction, $\gamma\gamma \to q\bar{q}$, which is exactly calculable in QED (direct or QPM component) and a "hard component" (resolved or anomalous or QCD component) which implies the knowledge of the quark and gluon density in the photon (Fig.1).

Two-photon collisions at high energies provide another experimental domain for testing of the QCD theory. A quasi-real photon interacts as a hadron due to quantum fluctuations into vector mesons or into quark-antiquark pairs. A consistent picture of hadron-hadron interaction should emerge from the studies of the $\gamma\gamma$, $\gamma p$, $ep$ and $pp$ collisions. The total $\gamma\gamma$

[†]on leave from Petersburg Nuclear Physics Institute, Gatchina, Russia.

cross section measurement gives an important verification of the expected universal high energy behaviour of the total hadron cross sections [1]. Diffractive quasi-elastic $\gamma\gamma \to \rho\rho$ scattering comprises sizable part of the total cross section and needs to be measured for better understanding of the energy flow in two-photon events. The measurement of charm production in two-photon collisions provides a good test of QCD, since perturbative calculations are expected to be reliable due to the large physical scale set by the charm quark mass. All together are important for a consistent description of the transition between soft and hard (low $p_t$ and high $p_t$) processes.

## 2 Total hadronic $\gamma\gamma$ cross section

The L3 detector has been described in detail in Ref. [2]. Hadronic two-photon events are selected by the following criteria Ref. [3]:

- At least six particles must be detected. A particle can be a track, a photon or other neutral cluster in the calorimeter.
- The total energy deposited in the calorimeters must be smaller than 50 GeV, to exclude annihilation events. The total energy in the electro-magnetic calorimeter is required to be greater than 500 MeV in order to suppress beam-gas and beam-wall backgrounds.
- We analyze the data corresponding to the scattering of the quasi-real photons (photon virtuality $Q^2 \approx 0$). An anti-tag condition is imposed which excludes events with electromagnetic clusters of energy greater than 50 GeV in the fiducial region of 33-64 mrad (L3 luminosity monitor).

The energy of a photon-photon collision is determined from the hadronic final state. The visible mass, $\mathrm{W_{vis}}$, of the event is calculated from the four-momentum vectors of the measured particles (tracks and calorimetric clusters). All particles are considered to be pions except for electromagnetic clusters identified as photons. The analysis is limited to events with $\mathrm{W_{vis}} > 5$ GeV. Data have been collected by L3 during 1997 at $\sqrt{s} = 183$ GeV with a total integrated luminosity of 51 $\mathrm{pb^{-1}}$. The number of selected events is 159012. The background (mainly the annihilation processes and $\gamma\gamma \to \tau\tau$) is below 1% and is subtracted from the data. The trigger efficiency, is determined directly from the data using a set of independent triggers. The trigger efficiency is mass dependent, it varies from (70±6)% at $W_{vis} = 5$ GeV to (88±2)% at $W_{vis} = 40$ GeV where it becomes constant.

The $\gamma\gamma \to hadrons$ processes (Fig.1) are simulated with the PHOJET [‡] [4] and PYTHIA [§] [5] event generators. For the annihilation processes $e^+e^- \to hadrons(\gamma)$, ZZ($\gamma$), Zee($\gamma$), We$\nu$($\gamma$) we have simulated events with PYTHIA [5], we have used KORALZ [6] for $e^+e^- \to \tau^+\tau^-(\gamma)$ and KORALW [7] for $e^+e^- \to W^+W^-$. For the $e^+e^- \to e^+e^-\tau^+\tau^-$ channel, events are simulated with DIAG36 [8]. The Monte Carlo predictions agree with the data, an example can be seen in Fig.2a and Fig.2b. PHOJET shows better agreement with the data.

From the number of events, corrected with the PHOJET Monte Carlo in each $W_{\gamma\gamma}$ bin, and the integrated luminosity, the cross section $d\sigma(e^+e^- \to e^+e^- hadrons)$ is measured. To extract the total cross section of two real photons the photon flux $\mathcal{L}_{\gamma\gamma}$ [9] is calculated and the hadronic two-photon processes are extrapolated to zero $\mathrm{Q^2}$. This is done by

[‡]PHOJET version1.05c
[§]PYTHIA version 5.718 and JETSET version 7.408

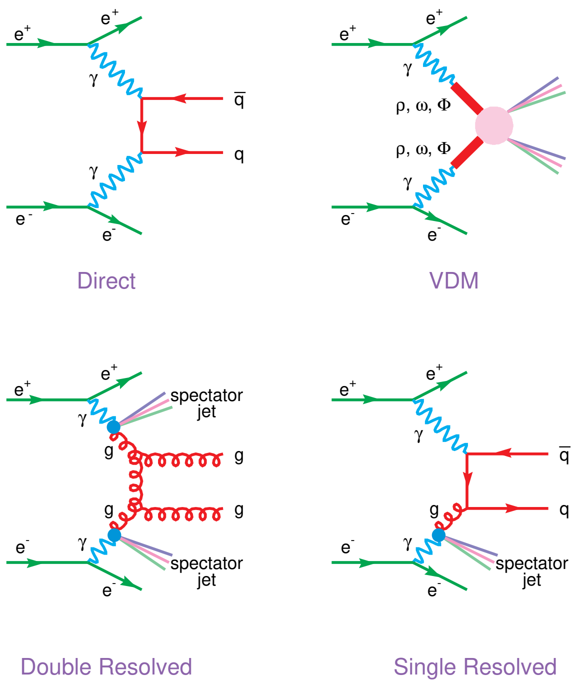


Figure 1: Production of hadrons in two-photon collisions at $e^+e^-$ colliders.

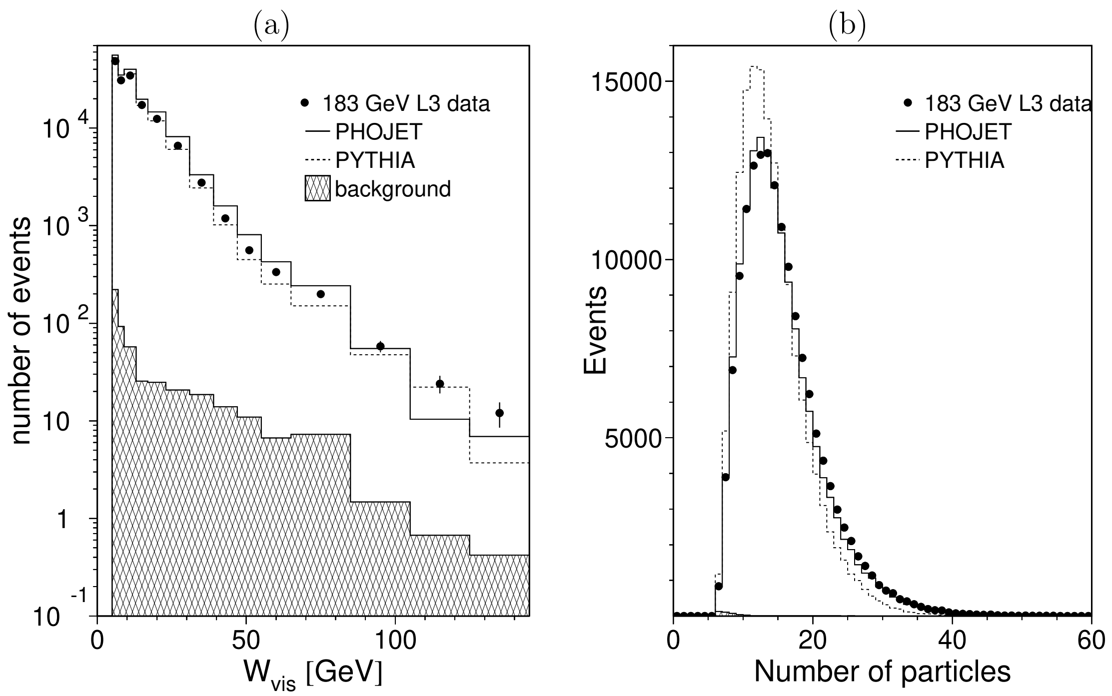


Figure 2: a)The measured visible mass at $\sqrt{s}$ = 183 GeV and b) the number of particles in the selected events, compared to PHOJET and PYTHIA expectations. The backgrounds are indicated as a shaded area.

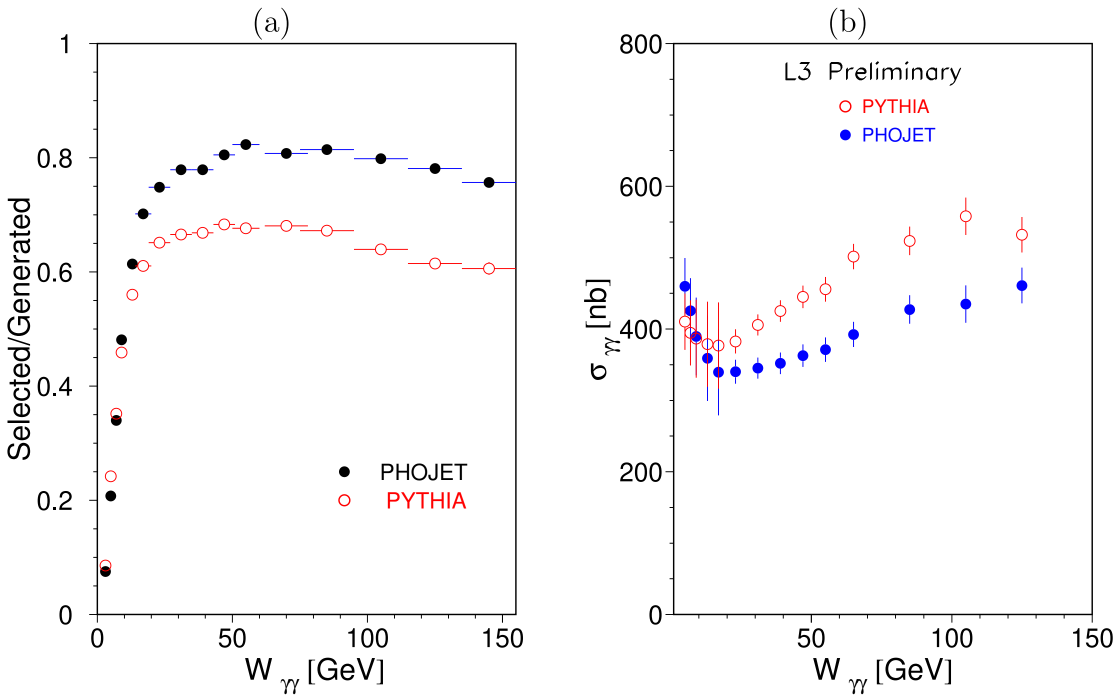


Figure 3: (a) Ratio of selected over generated events as a function of the two-photon mass, as calculated by the two generators PHOJET and PYTHIA. b) The two-photon total cross section obtained by correcting the data with PHOJET (full points) and by PYTHIA (open points). The errors are statistical and systematic added in quadrature.

considering the dominant transverse photon (T) interaction as well as the small scalar photon (S) contribution [10] :

$$d\sigma(e^+e^- \rightarrow e^+e^- hadrons)/dW_{\gamma\gamma} = \int \frac{d(Q_1^2)}{Q_1^2}\frac{d(Q_2^2)}{Q_2^2} \sum_{a,b=T,S} \mathcal{L}_{ab}\sigma_{ab}(W_{\gamma\gamma}, Q_1^2, Q_2^2). \quad (1)$$

The $W_{\gamma\gamma}$ and $Q^2$ dependencies of the cross section can be factorized for $Q^2 << W^2_{\gamma\gamma}$ :

$$\sigma_{a,b}(W_{\gamma\gamma}, Q_1^2, Q_2^2) = F_a(Q_1^2)F_b(Q_2^2)\sigma_{\gamma\gamma}(W_{\gamma\gamma}, 0., 0.) \quad (2)$$

For each $W_{\gamma\gamma}$ bin a numerical integration is performed over the unmeasured $Q^2$ of the scattered electron or positron. A model [11] has been used for the form factors $F(Q^2)$. Depending on the form factors used, the extracted values of cross section may vary by $\pm 5\%$ [10], independent of $W_{\gamma\gamma}$ in the studied mass range. The true two-photon invariant mass $W_{\gamma\gamma}$ is obtained from the visible hadron mass $W_{vis}$ using an unfolding procedure [12]. After unfolding, the events are corrected for detector acceptance and efficiency in each $W_{\gamma\gamma}$ interval (Fig.3a). The low acceptance below $W_{\gamma\gamma} = 30$ GeV is due to the $W_{vis}$ cutoff of 5 GeV . For $W_{\gamma\gamma} > 30$ GeV, the acceptance is rather flat, but there is a systematic difference of $\simeq 20\%$ between the two Monte Carlo models. This is due to a different modeling of the diffractive events.

The mass dependent statistical and systematic errors are added in quadrature. The uncertainty related to the Monte Carlo model are not added to the systematic errors, but the complete analysis is done for PYTHIA as well as for PHOJET (Fig.3b). The discrepancy on the cross section reflects the difference on selection efficiency given by the two generators. The measurement is compatible within errors with our previous measurements at $\sqrt{s} = 133$ GeV and $\sqrt{s} = 161$ GeV [13], extends the range of accessed $W_{\gamma\gamma}$ energies and is consistent with preliminary results of OPAL [14].

The data show characteristic total hadronic cross section behaviour – a steep decrease at low $W_{\gamma\gamma}$ energy and a slow rise at high energies. This behaviour corresponds to the exchange of Regge trajectories (Reggeon exchange for low energy region and the Pomeron exchange at high energies). A parametrisation by A.Donnachie and P.V. Landshoff [15] of the form

$$\sigma_{\rm tot} = A\, s^{\epsilon} \,+\, B\, s^{-\eta} \tag{3}$$

describes well the energy behaviour of all total cross sections. The coefficients $A$ and $B$ are process and $Q^2$ dependent, while the powers of $s$ being universal. The data are fitted to Eq. 3 with the parameters $\epsilon$ and $\eta$ fixed to the world average value ($\epsilon = 0.0790 \pm 0.0011$ and $\eta = 0.4678 \pm 0.0059$ [16]). The fit is shown in Fig.4a together with the Reggeon and the Pomeron components. The fit with the fixed $\epsilon$ parameter does not agree well with the observed rise of the $\sigma_{\gamma\gamma}$ cross section. Taking into account only statistical errors gives $\chi^2 = 348$ for 12 degrees of freedom, value which drops to $\chi^2 = 11$ by taking into account also the systematic errors. A fit with A, B and $\epsilon$ as free parameters (Fig.4b) gives:

$\epsilon = 0.158 \pm 0.006(\text{stat}) \pm 0.028(\text{sys})$ using data corrected with PHOJET
$\epsilon = 0.143 \pm 0.005(\text{stat}) \pm 0.025(\text{sys})$ using data corrected with PYTHIA

This value is about a factor two higher than the universal value [16], independent on the Monte Carlo model used to correct the data.

The two-photon cross section at high energies can be estimated from proton-proton and photoproduction total cross sections assuming factorization for the Pomeron term [17]:

$$\sigma_{\gamma\gamma} \approx \sigma^2_{\gamma\rm p}/\sigma_{\rm pp} \tag{4}$$

To compare our data to this factorization prediction, we perform the same Regge fit, keeping $\epsilon$ and $\eta$ fixed, to the photoproduction data [18] and we calculate the coefficients $\mathrm{A}_{\gamma\gamma}=\mathrm{A}^2_{\gamma\rm p}/\ \mathrm{A}_{\rm pp}$ and $\mathrm{B}_{\gamma\gamma}=\mathrm{B}^2_{\gamma\rm p}/\mathrm{B}_{\rm pp}$. The predictions thus obtained are consistent with the two-photon measurement (Fig.4c).

In Fig.4d the predictions from several QCD inspired models are shown.

The model of G.A. Schuler and T. Sjöstrand [19] aims at a smooth superposition of hadron-like and point-like photon interactions. Following their prediction, one sees that the fluctuation of both photons into vector mesons is not sufficient to describe the data (lower, dashed-line in Fig.4d). Adding the point-like splitting of the photon to $\mathrm{q\bar{q}}$ pairs, the cross section increases to values comparable to our data points. The maximum QCD contribution, allowed by unitarity, is indicated by the higher dashed-line in Fig.4d.

The cross sections predicted by R.Engel and J.Ranft [4] (dotted-line in Fig.4d) are in agreement with the data corrected with PHOJET. In their model $\gamma$p and pp data are used to fix the couplings of the Pomeron and of the Reggeon to the $\mathrm{q\bar{q}}$ fluctuation of the photon. The cross sections are then calculated in the framework of a Dual Parton Model with the unitarization constraint, the prediction has an accuracy of $\pm 10\%$ [4].

The calculation of the mini-jet model of R.M.Godbole and G.Pancheri [20] is also shown in Fig.4d as a solid line. The calculation depends on the choice of the lowest transverse momentum (2 GeV) used in the hard jet cross section calculation and on the parameter $k_0$ which defines intrinsic parton $p_t$ distribution in the photon.

The predictions of the QCD driven models are in a qualitative agreement with the data.

Modifications to the parametrization of the total cross section were recently proposed by A.Donnachie and P.V. Landshof [21] in order to allow bigger slope of high energy part by the admixture of the 'hard' Pomeron to the 'soft' one. This might be just phenomenological parametrization as the next to leading order corrections to the BFKL Pomeron exchange were found to be very large [22] , thus the prediction for the slope of the BFKL Pomeron is uncertain.

# 3 The reaction $e^+e^- \rightarrow \rho^0\rho^0$

Since photons can fluctuate directly into neutral Vector Mesons, the $\gamma\gamma \rightarrow \rho^0\rho^0$ cross-section is expected to remain large at high $\gamma\gamma$ centre-of-mass energies [23] ("elastic" $\gamma\gamma$ scattering).

The exclusive $e^+e^- \rightarrow e^+e^-\pi^+\pi^-\pi^+\pi^-$ events are selected by requiring four tracks, each with the distance of closest approach to the average position of the e$^+$e$^-$ collision point in the r-$\phi$ plane be less than 1 mm, the sum of charges be equal to zero and missing transverse momentum squared smaller than 0.05 GeV$^2$. At $\sqrt{s} = 183$ GeV this requirement selects 6290 events. The $\gamma\gamma \rightarrow 4\pi$ cross section is evaluated by correcting the data for acceptance and efficiency ¶ and by using the Low [25] formula for the two-photon luminosity function. The values thus obtained, shown in Fig.5a, agree well with previous measurements [26].

There are 236 events with a mass $W_{\gamma\gamma} > 3$ GeV. Fig.5b shows the $\pi^+\pi^-$ mass distribution after the combinatorial background subtraction. The background is estimated with wrong sign combinations. The events are compared to the expectations of PYTHIA and PHOJET. The data sample contains only a small visible $\rho^0\rho^0$ peak similar to PHOJET. PYTHIA seems to overestimate the quasi-elastic component of the $\gamma\gamma$ cross section. The scatter plot of the masses of the neutral combinations of two pions is shown in Fig.5c. To improve visibility the histograms were symmetrized. The expected very good separation between the signal and the combinatorial background can be clearly seen from the Pythia $\rho^0\rho^0$ sample. The $W_{\gamma\gamma}$ distribution of the $4\pi$ events is shown in Fig.5d. This distribution is better described by PHOJET than by PYTHIA. While PHOJET in average is too high by approximately 20 %, it correctly describes the shape of the distribution. PYTHIA contains too many high mass events, mainly due to large $\rho^0\rho^0$ contribution.

# 4 Charm production cross section

The production of heavy quarks in two-photon collisions consists mainly of charm quarks. Because of their smaller electric charge and larger mass, the production of b-quarks is expected to be suppressed by more than two orders of magnitude relative to the production of charm quarks [27]. At high energies, the direct and resolved processes (Figure 1) are predicted to give comparable contributions to the cross section [27]. The contribution to charm production from soft processes described by the Vector Dominance Model (VDM) is expected to be small at LEP energies. The single-resolved photon cross section is

¶The PC Monte Carlo [24] is used which generates the decays $X \rightarrow \rho^0\rho^0$ and $\rho^0 \rightarrow \pi^+\pi^-$ uniformly in the two-body phase space

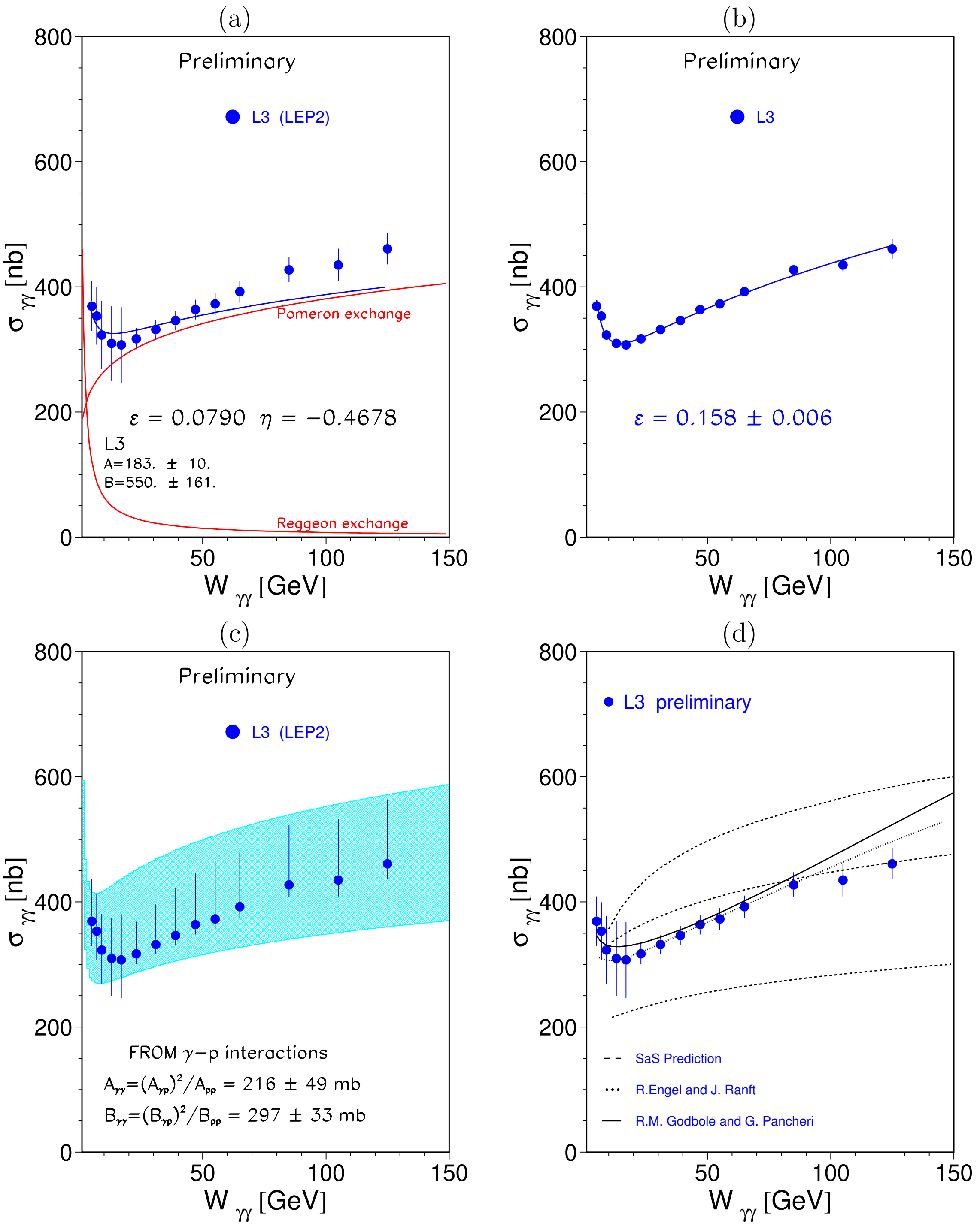


Figure 4: a) Total cross section $\gamma\gamma \to hadrons$ obtained by correcting the data with PHOJET. The errors are statistical and systematic added in quadrature. The continuous line is the Regge fit, with fixed values of $\epsilon$ and $\eta$ described in the text. The two components : the rapidly decreasing Reggeon part and the slowly rising component due to Pomeron exchange are indicated. b) The factorization predictions (grey area) from proton-proton and photoproduction data are compared to the measured two-photon values. Here the upper error bar indicates the values obtained by correcting the data with PYTHIA. c)Regge fit to the two-photon total cross section with $\epsilon$ left as free parameter, only the statistical errors are indicated. d) Comparison with QCD inspired models, see text.

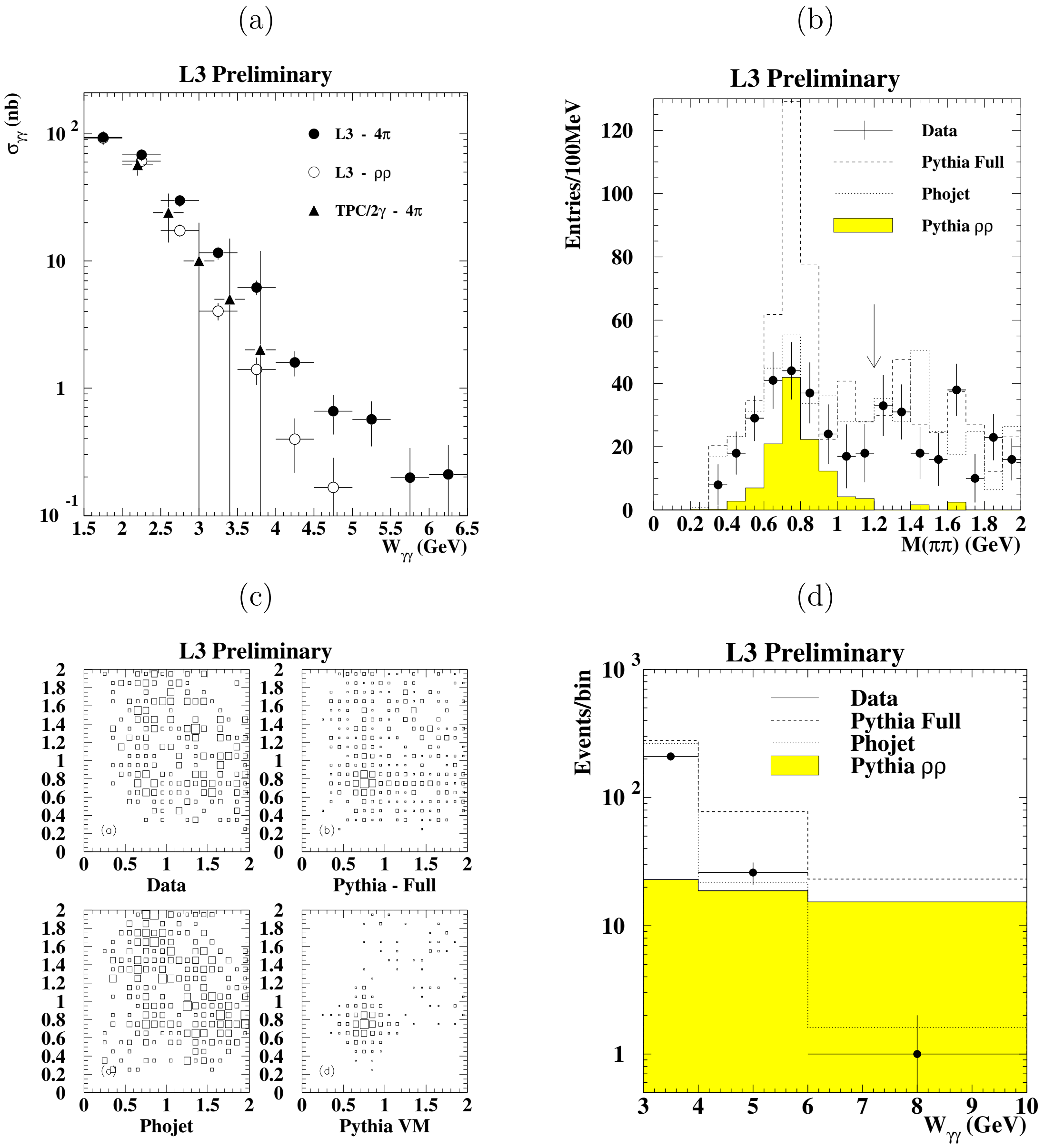


Figure 5: a)The cross section $\gamma\gamma \rightarrow 4\pi$ as a function of $W_{\gamma\gamma}$ , measured at $\sqrt{s} = 183$ GeV, compared to TPC/2$\gamma$ results. b) Effective mass of two oppositely charged pions, after subtraction of background estimated from wrong sign combinations. The dotted line is the expectation of PHOJET, the dashed line the one of PYTHIA, the shaded area is the contribution from elastic $\rho^0\rho^0$ production in PYTHIA. c)Scatter plot of the two $\pi^+\pi^-$ mass combinations, after subtraction of background from wrong combinations. The data distribution is compared to PHOJET, PYTHIA and the $\rho^0\rho^0$ PYTHIA distributions. For each event the two neutral combinations are added and the one with wrong charge subtracted from the symmetrized histograms. d) Number of $4\pi$ events as a function of $W_{\gamma\gamma}$. The data are compared to Monte Carlo predictions. The shaded histogram is the PYTHIA $\rho^0\rho^0$ prediction.

dominated by the photon-gluon fusion diagram $\gamma g \rightarrow c\bar{c}$. The production rate of the charm quarks in two-photon collisions depends on the mass of the charm quark and on the gluon density in the photon. Precise measurements of the process $\gamma\gamma \rightarrow c\bar{c}$ constrain thus these physical parameters. Measurements of charm production in two-photon collisions were done at PEP, PETRA, TRISTAN and LEP1 energies [28–34], where charm was tagged by charged $D^*$ mesons, inclusive leptons (electrons and muons) and $K^0_S$ mesons.

In this paper we present the result of the measurement of the $e^+e^- \rightarrow e^+e^- c\bar{c}X$ cross section by the L3 experiment at $\sqrt{s} = 91$ GeV (LEP1) and at energies higher than the Z mass (LEP2). We identify charm quarks by tagging electrons and muons from semi-leptonic charm decays. The data collected by L3 in the period of 1994 through 1997 at $\sqrt{s} = 91$-$183$ GeV have been analyzed for a total integrated luminosity of $\mathcal{L} = 165$ pb$^{-1}$. For the first time the charm production cross section is measured at more than one energy in a single experiment.

The event selection is done in two steps. The first one selects hadronic final states produced in two-photon collisions, and the second identifies a charm quark. Hadronic two-photon events are selected by cuts on the number of tracks, the visible energy and the visible mass. We require at least five tracks in each event, the visible energy has to be less than $0.38\sqrt{s}$ and the visible mass has to be greater than 3 GeV. The analysis is limited to untagged events with small photon virtuality. Events are excluded when the most energetic cluster in the L3 luminosity monitor has an energy greater than $0.4\,E_{beam}$. The number of events selected at different energies is given in Table 1. After the hadron selection, the background from the annihilation processes and the two-photon production of tau pairs is about 2% at LEP1 and is below 1% at higher energies.

To tag charm-quark production, we search for an electron with momentum greater than 0.6 GeV in polar angle range $|\cos\theta| < 0.9$. Electron candidates are selected as follows:

- The electromagnetic calorimeter cluster matches to a track: the difference between the azimuthal angles estimated from the shower barycentre and from the track impact point at the calorimeter must be smaller than 20 mrad. The shower shape must be compatible with the expectation ($\chi^2$ test).
- The cluster, matched to a track, must also satisfy the condition $0.85 < E_t/p_t < 1.20$ (Figure 6), where $E_t$ is the projection of the energy of the cluster on the r-$\phi$ plane and $p_t$ is the transverse momentum of the track. The ratio, $E_t/p_t$, has the power to reject more than 95% of the hadrons (mainly pions) while keeping more than 90% of the electrons for which the expected value is near unity.
- The distance of closest approach of the track to the average position of the $e^+e^-$ collision point in the r-$\phi$ plane must be less than 0.5 mm.

The number of selected events, after all cuts are applied, are given in Table 1. The trigger efficiencies range from 87% at $\sqrt{s} = 91$ GeV to 79% at $\sqrt{s} = 183$ GeV. The background from the annihilation processes and the two-photon production of tau pairs is 10% at $\sqrt{s} = 91$ GeV and is about 1% at higher energies. The electron selection efficiency is about 10%; the electron identification probability is 85%. Both fractions are estimated using the PYTHIA Monte Carlo.

In Figure 7, the inclusive electron cross section at 183 GeV is plotted as a function of the transverse momentum of the electron. The prediction from the PYTHIA Monte Carlo

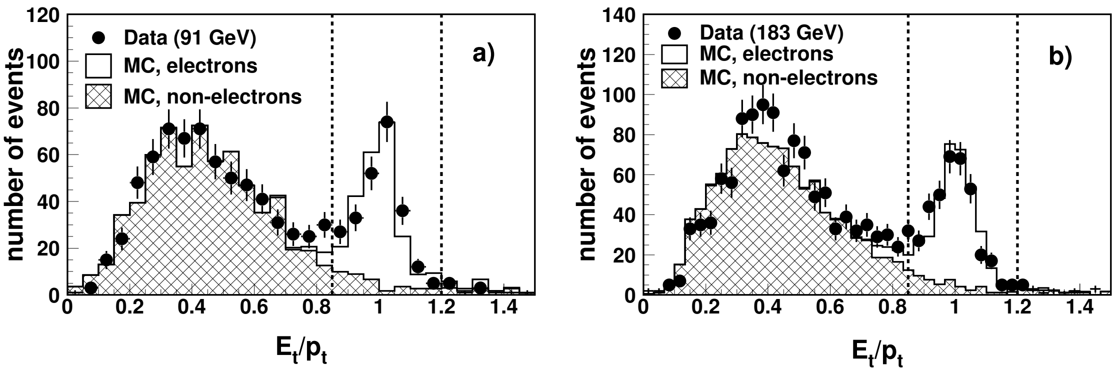


Figure 6: The ratio, $E_t/p_t$, of the transverse energy measured by the electromagnetic calorimeter and the transverse momentum of the track for a) $\sqrt{s} = 91$ GeV and b) $\sqrt{s} = 183$ GeV. A clear electron signal is observed at the expected value of $E_t/p_t = 1$. A window, defined by the dashed lines, of $0.85 < E_t/p_t < 1.2$ selects the electron candidates.

| $\sqrt{s}$ [GeV] | $\mathcal{L}$ [pb$^{-1}$] | Hadronic Events | Electron Tag Events | Muon Tag Events |
|---|---|---|---|---|
| 91 | 79.8 | 93204 | 282 | 57 |
| 130 – 140 | 12.1 | 21045 | 82 | – |
| 161 – 172 | 21.2 | 44444 | 156 | 16 |
| 183 | 52.2 | 116760 | 433 | 52 |

Table 1: Data samples collected by L3 in the period of 1994 through 1997 at $\sqrt{s} = 91$-183 GeV and the corresponding integrated luminosities $\mathcal{L}$.

for inclusive charm production and background is also plotted. The background from misidentified electrons and from $\gamma$-conversions (this background comprises about 22% of the selected electron sample) is subtracted bin by bin. The prediction is normalized to the number of events in the data, the predicted number of events is about 60% too small (about 10% too small at LEP1 energy). The shape of the distribution is in agreement with the prediction. Leptons from semi-leptonic decays of charm quarks are on average more energetic than leptons from background two-photon processes, therefore, the charm purity increases with the transverse momentum.

The muon candidate is required with momentum greater than 2 GeV as only such muons can penetrate through the calorimeters to reach the muon chambers. In order to suppress the contribution from the annihilation processes, we require the muon momentum to be less than 0.2 $E_{beam}$. The angular acceptance is limited to $|\cos\theta| < 0.9$. After all cuts are applied, 57, 16 and 52 events remain at the center of mass energies $\sqrt{s} = 91$ GeV, 167 GeV and 183 GeV, respectively. The trigger efficiency is higher by a factor 1.08 than in the case of electron selection due to the higher momentum cut. The background from annihilation processes and two-photon production of tau pairs is 24% at $\sqrt{s} = 91$ GeV and is about 5% at higher energies.

The total cross section of inclusive charm production is calculated from the following equation:

$$\sigma = \frac{(N_{obs} - N_{bkg})\ \pi_{charm}}{\mathcal{L}\ \epsilon_{trig}\ \epsilon_{charm}} \quad (5)$$

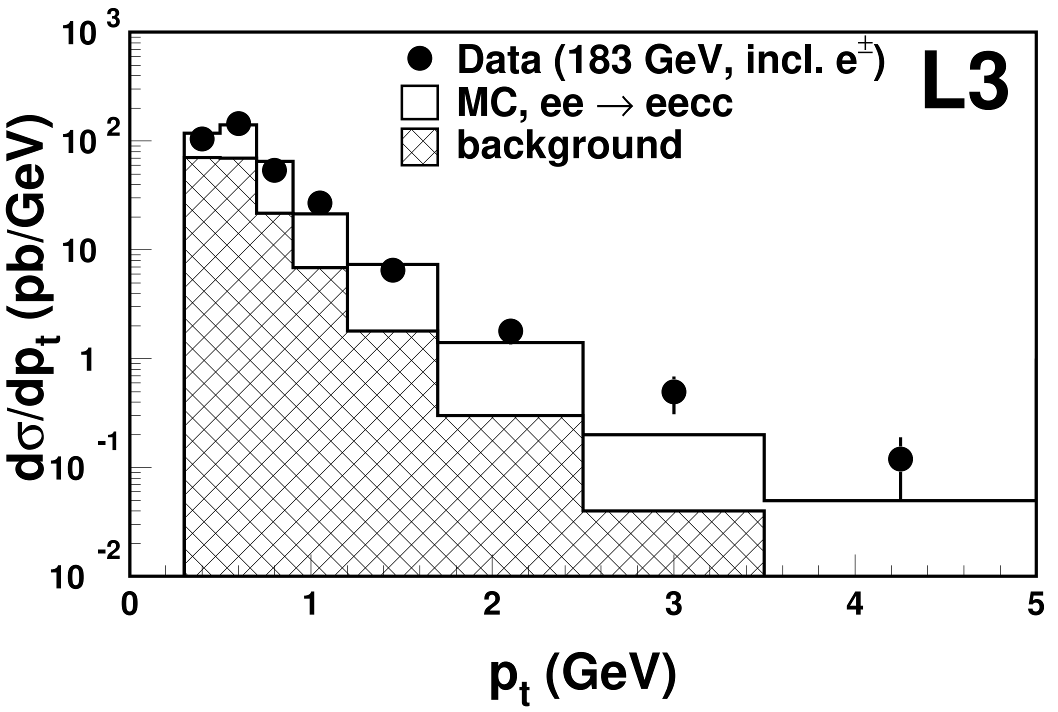


Figure 7: The differential cross section as a function of the electron transverse momentum. The data are compared to the Monte Carlo prediction for charm production and for the background. The Monte Carlo prediction is normalized to the number of events in the data.

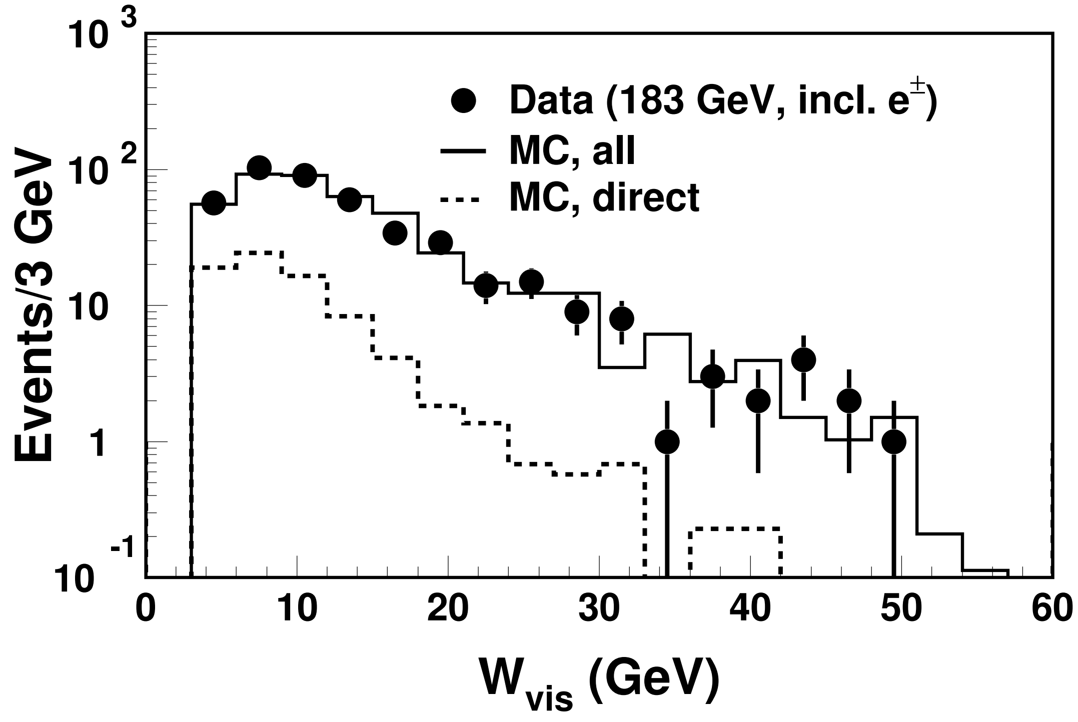


Figure 8: Comparison of the visible mass spectra for the electron data at $\sqrt{s} = 183$ GeV to that from PYTHIA events generated with massless matrix elements. The Monte Carlo spectra are normalized to the same number of events as the data. The dashed histogram is the contribution from the direct process.

The charm selection efficiency, $\epsilon_{\rm charm}$, is the fraction of charm events selected by the lepton tag analysis relative to the events generated in the full phase space. The charm purity, $\pi_{\rm charm}$, is defined as:

$$\pi_{charm} = \frac{N_c}{N_c + N_{nc}} \tag{6}$$

In order to be less dependent on the Monte Carlo prediction, the charm purity is calculated from the efficiencies to select two-photon, charm and non-charm events after hadronic selection was done:

$$\pi_{charm} = \frac{1 - \frac{\epsilon_{nc}}{\epsilon_{\gamma\gamma}}}{1 - \frac{\epsilon_{nc}}{\epsilon_c}} \tag{7}$$

The selection efficiency of hadronic two-photon events, $\epsilon_{\gamma\gamma}$, is defined as

$$\epsilon_{\gamma\gamma} = \frac{(N_{obs} - N_{bkg})}{(N_{obs} - N_{bkg})_{hadronic\ selection}} \tag{8}$$

This selection efficiency is calculated directly from the data. The efficiency $\epsilon_{\rm c}$ ($\epsilon_{\rm nc}$) is the ratio of the number of charm $\rm N_c$ (non-charm $\rm N_{nc}$) events, selected with all cuts applied, to the number of charm (non-charm) events at the hadronic selection level.

The expression for the purity $\pi_{charm}$ can be derived from the equation for the number of hadronic selected events, namely

$$\frac{N_c + N_{nc}}{\epsilon_{\gamma\gamma}} = \frac{N_c}{\epsilon_c} + \frac{N_{nc}}{\epsilon_{nc}} \tag{9}$$

The charm purity calculated this way does not rely on the generated Monte Carlo sample composition (charm versus non-charm). The charm purity is about 60% for electrons and about 65% for muons. For the electron tag, the charm selection efficiency increases from 0.44% at $\sqrt{\rm s} = 91$ GeV to 0.53% at $\sqrt{\rm s} = 183$ GeV. This efficiency is much lower for the muon tag, about 0.05% at all energies, due to the higher momentum cut. The cross sections are given in Table 2 with the statistical and systematic uncertainties. Systematic errors arise from the uncertainty on background subtraction, selection efficiencies, trigger efficiency and cut variation.

The charm production cross sections are obtained with the PYTHIA Monte Carlo using a massless quark matrix element calculation. The effect of the use of massive matrix elements is tested by using the PYTHIA Monte Carlo events generated with the charm mass $\rm m_c = 1.6$ GeV. Since the cross section values are dependent on the ratio of the charm purity to the charm selection efficiency, $\pi_{\rm charm}/\epsilon_{\rm charm}$, we compare the value of this ratio using the massless matrix elements to the ratios obtained from the massive approach. The difference falls within the statistical uncertainty for both the electron and the muon selection.

The PYTHIA Monte Carlo is the only generator available which includes all of the hadronic two-photon processes relevant in this analysis. The exact QED JAMVG [35] program generates only the direct process. To better understand possible systematics due to the different models, we have compared the values of $\pi_{\rm charm}/\epsilon_{\rm charm}$ for the direct process as given by PYTHIA and by JAMVG. There is agreement within 10%, comparable with the statistical uncertainty. However, in the case of the electron tag, the value of $\pi_{charm}/\epsilon_{charm}$ for the direct process is two times higher than that for the resolved process.

The most sensitive distributions where predictions for direct and resolved processes are different are found to be the visible mass, the track multiplicity, the transverse momentum

| $\sqrt{s}$ [GeV] | Electron Tag $\sigma$ [pb] | Muon Tag $\sigma$ [pb] | Combined $\sigma$ [pb] |
|---|---|---|---|
| 91 | $435 \pm 64 \pm 75$ | $601 \pm 168 \pm 163$ | $458 \pm 60 \pm 70$ |
| 133 | $1358 \pm 243 \pm 180$ | – | $1358 \pm 243 \pm 180$ |
| 167 | $1009 \pm 152 \pm 106$ | $576 \pm 361 \pm 188$ | $944 \pm 140 \pm 95$ |
| 183 | $1291 \pm 105 \pm 116$ | $1260 \pm 328 \pm 243$ | $1288 \pm 100 \pm 107$ |

Table 2: Total cross section values for process $e^+e^- \to e^+e^-c\bar{c}X$ at four different LEP energies using electron and muon tags. The statistical and systematic uncertainties are also given. In the last column, the data from both lepton tags are combined.

of the lepton and the energy flow spectra [36]. A comparison of the visible mass data distribution with the expectations of the direct only and the all two-photon processes for the high statistics electron sample at $\sqrt{s} = 183$ GeV is given in Figure 8. The direct process decreases more quickly than the resolved process with visible mass.

The total inclusive charm production cross sections are plotted in Figure 9 together with previous measurements [28–34]. For the purpose of comparison, the published results of different experiments were extrapolated to the total charm cross sections using the procedure of Ref. [37]. The data are compared to the theory predictions of Ref. [27]. The dashed line corresponds to the direct process, NLO QCD calculation, while the solid line shows the QCD prediction for the sum of the direct and the resolved processes calculated to NLO accuracy. The theoretical prediction is calculated using a charm mass of 1.3 GeV; the open charm threshold energy is set to 3.8 GeV. The theory prediction for the resolved process was calculated with the parton density function of Glück-Reya-Vogt [38]. Using the Drees-Grassie [39] parametrization for the photon parton density results in a decrease of the cross section of 3% for $m_c = 1.7$ GeV and of 9% for $m_c = 1.3$ GeV. The renormalization scale was chosen to be the charm mass. A change in the renormalization scale from $m_c$ to $2m_c$ decreases the QCD prediction by 30% (15%) for $m_c = 1.3$ (1.7) GeV. The theoretical uncertainties in the calculations indicate that it is not possible to determine the mass of the charm quark simply by measuring the total charm cross section. However, the direct process is only dependent upon the heavy-quark mass and the QCD coupling constant. With further study of the differential distributions and increased statistics, we may be able to isolate the direct process contribution thus obtaining a measurement of the charm quark mass.

# 5 Summary

The cross section $\sigma(\gamma\gamma \to hadrons)$ has been measured in the interval $5 \leq W_{\gamma\gamma} \leq 145$ GeV. The observed slope of the rise of the $\sigma(\gamma\gamma \to hadrons)$ with energy is by factor two bigger than expected from the universal Regge behaviour of total hadronic cross sections. The diffractive production of the two $\rho^0$ mesons $\gamma\gamma \to \rho^0\rho^0$ is also studied.

The cross section for inclusive charm production in two-photon collisions, $\sigma(e^+e^- \to e^+e^-c\bar{c}X)$, is measured with the L3 detector at 91 GeV $\leq \sqrt{s} \leq$ 183 GeV. The cross section increases with energy as expected by QCD predictions. The direct process $\gamma\gamma \to c\bar{c}$ is insufficient to describe the data, even including real and virtual gluon corrections. The cross section values and the event distributions require contributions from the

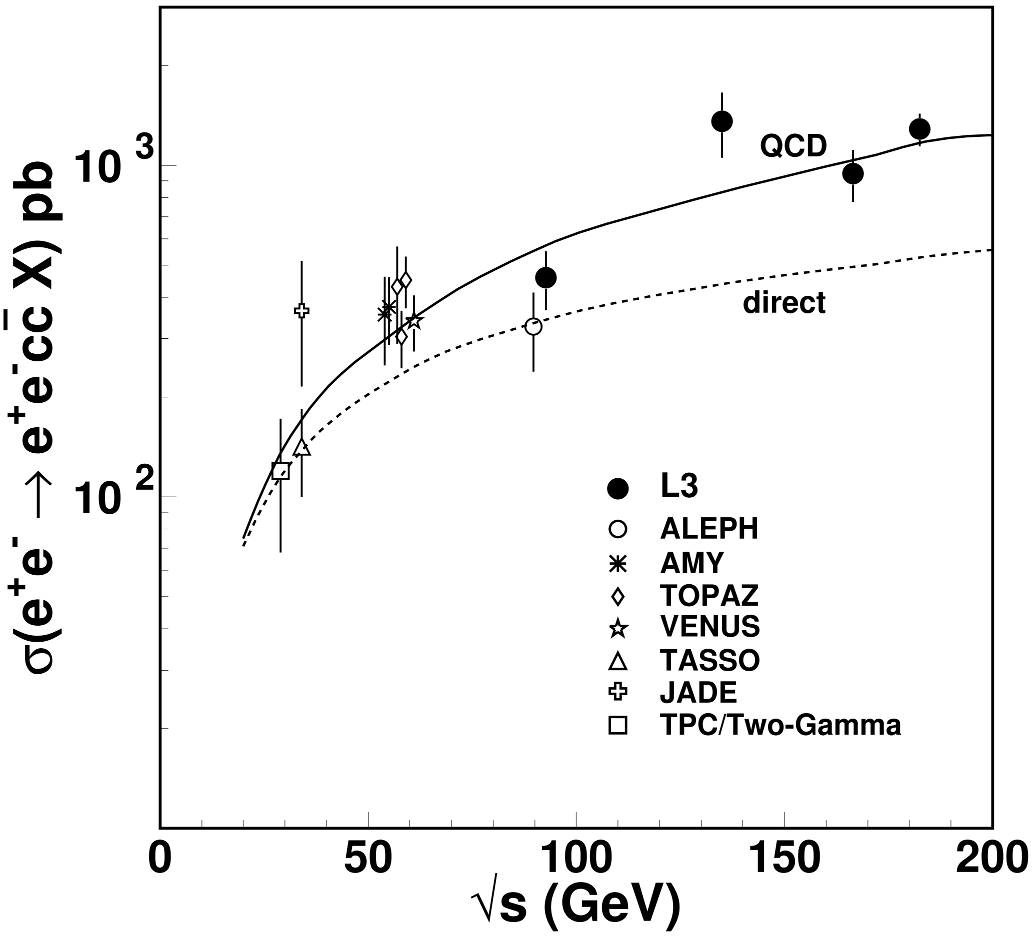


Figure 9: The charm production cross section in two-photon collisions. The L3 data from both the electron and the muon tags have been combined. The statistical and systematic errors are added in quadrature. The dashed line corresponds to the direct process prediction while solid line shows the QCD prediction for the sum of the direct and the resolved processes calculated to the NLO accuracy [27]. The prediction corresponds to a calculation for a charm mass of 1.3 GeV, the parton density function of Glück-Reya-Vogt [38] and the renormalization scale was chosen to be the charm mass. The points at TRISTAN and LEP1 energies were artificially separated to avoid merging.

resolved processes which are dominantly $\gamma g \rightarrow c\bar{c}$. The data are therefore sensitive to the gluon density in the photon.

# Acknowledgements

I wish to thank G.Jarlskog for organizing of interesting and pleasant workshop. I wish to thank my colleagues of the L3 two-photon physics group for the collaboration, in particular, Lotfi Fredj for the help in the preparation of plots and Roger McNeil for careful reading of the manuscript. I would like to thank Alex Finch and Michael Krämer for providing us with the source code for the charm cross section calculation.

## References

[1] Review of Particle Physics, Eur. Phys. J. **C 3**(1998) 1.

[2] L3 Collaboration, B. Adeva *et al.*, Nucl. Instr. and Meth. **A 289** (1990) 35;
L3 Collaboration, O. Adriani *et al.*, Phys. Rep. **236** (1993) 1.

[3] L3 Collaboration, M. Acciari *et al.*, paper 519 of the 29th Intern. Conf. on High-Energy Physics, Vancouver, Canada (1998).

[4] R. Engel, Z. Phys. **C 66** (1995) 203 ;
R. Engel and J. Ranft, Phys. Rev. **D 54** (1996) 4246;
And R. Engel private communication.

[5] T. Sjöstrand, Comput. Phys. Commun. **82** (1994) 74.

[6] S. Jadach, B.F.L. Ward and Z. Was, Comput. Phys. Commun. **79** (1994) 503.

[7] M. Skrzypek, S. Jadach, W. Placzek and Z. Was, Comput. Phys. Commun. **94** (1996) 216.

[8] F.A. Berends, P.H. Daverveldt and R.Kleiss, Nucl. Phys. **B 253** (1985) 441.

[9] V.M. Budnev, I.F. Ginzburg, G.V. Meledin and V.G. Serbo, Phys.Rep. **C 15** (1974) 181.

[10] G.A. Schuler, hep-ph/9610406, CERN-TH/96-297.

[11] J.J. Sakurai and D. Schildknecht, Phys. Lett. **B 40** (1972) 121.

[12] G. D'Agostini, Nucl. Instr. and Meth. **A 362** (1995) 487.

[13] L3 Coll., M. Acciari et al., Phys. Lett. **B 408** (1997) 450.

[14] OPAL Coll., paper 199 of the 29th Intern. Conf. on High-Energy Physics, Vancouver, Canada (1998);
S. Söldner-Rembold, Proc. of ICHEP98, hep-ex 9810011.

[15] A. Donnachie and P.V. Landshoff, Phys. Lett. **B 296** (1992) 227.

[16] Review of Particle Physics, Phys. Rev. **D 54** (1996) 192.

[17] V.N. Gribov and I.Ya. Pomeranchuk, Phys. Rev. Lett.**8** (1962) 343;
S.J. Brodsky, J.Phys.Suppl. (Paris) **35** (1974) C2-69;
K.V.L. Sarma and V. Singh , Phys. Lett. **B 101** (1981) 201.

[18] Zeus Coll., M. Derrick et al., Z. Phys. **C 63** (1994) 391.
H1 Coll.,S. Aid et al., Z. Phys. **C 69** (1995) 27.
and data files of the COMPAS Group, IHEP, Protvino.

[19] G.A. Schuler and T. Sjöstrand, Nucl. Phys. **B 407** (1993) 539 ;
G.A. Schuler and T. Sjöstrand, Z. Phys. **C 73** (1997) 677.

[20] R.M. Godbole and G. Pancheri, these proceedings.

[21] A. Donnachie and P.V. Landshoff, hep-ph 9806344.

[22] V.S. Fadin and L.N. Lipatov, Phys. Lett. **B 429** (1998) 127.

[23] V.L. Chernyak and I.R. Zhitnitsky, Nucl. Phys. **B 222** (1983) 382.

[24] F.L. Linde, Charm production in two-photon collisions, Ph.D. Thesis (Rijksuniversiteit Leiden,1988).

[25] F. Low, Phys. Rev. **120** (1960) 582.

[26] TPC/2$\gamma$ Coll., H. Aihara et al., Phys. Rev. **D 37** (1988) 28.

[27] M. Drees, M. Krämer, J. Zunft and P.M. Zerwas, Phys. Lett. B **306**, 371 (1993).

[28] JADE Collab., W. Bartel et al., Phys. Lett. B **184**, 288 (1987).

[29] TPC/Two-Gamma Collab., M. Alston-Garnjost et al., Phys. Lett. B **252**, 499 (1990).

[30] TASSO Collab., W. Braunschweig et al., Z. Phys. C **47**, 499 (1990).

[31] TOPAZ Collab., R. Enomoto et al., Phys. Lett. B **328**, 535 (1994), Phys. Rev. D **50**, 1879 (1994), Phys. Lett. B **341**, 99 (1994), Phys. Lett. B **341**, 341 (1994).

[32] VENUS Collab., S. Uehara et al., Z. Phys. C **63**, 213 (1994).

[33] T. Nozaki (AMY Collab.), in Proceedings of PHOTON 95, Sheffield (1995), S. Cartwright, D. Miller and V.A. Khose *eds* (World Scientific).

[34] ALEPH Collab., D. Buskulic et al., Phys. Lett. B **355**, 595 (1995).

[35] J.A.M. Vermaseren, Nucl. Phys. B **229**, 347 (1983).

[36] V.P. Andreev, R.R. McNeil and A.L. Stone, L3 Note 2263 (1998). This L3 Note is available on request from: The L3 secretariat, CERN, CH-1211 Geneva 23, Switzerland. Internet: http://l3www.cern.ch

[37] M. Cacciari et al., in CERN 96-01 Physics at LEP2, edited by G. Altarelli, (1996), v.1, p. 334.

[38] M. Glück, E. Reya and A. Vogt, Phys. Rev. D **46**, 1973 (1992).

[39] M. Drees and K. Grassie, Z. Phys. C **28**, 451 (1985).